IRAQI BULLETIN OF GEOLOGY AND MINING (IBGM)\
IRAQ GEOLOGICAL SURVEY (GEOSURV-IRAQ)

*IBGM (**2025**, Vol 21; Issue 2)* *251-273*

GEOLOGICAL STRUCTURE AND BASEMENT DEPTH OF THE BUSAIYA SUB-BASIN, SW IRAQ, USING GEOPHYSICAL AND REMOTE SENSING METHODS

Hayder Al-Bahadily[1 *], James Fairhead[2], Hanbing Ai[3], Younus Al-Saady[1], Ahmad Mousa[1] and Yasir Shyaa[4]

[1] Department of Geology, Geophysics Division, Iraq Geological Survey, Baghdad, Iraq
[2] School of Earth and Environment, University of LEEDS, UK
[3] School of Geophysics and Geomatics, China University of Geosciences, China
Oil Exploration Company, Baghdad, Iraq [4]
[*] Correspondence: hayder.adnan17@gmail.com

Type of the Paper (Article)
Received: 04/02/2025
Accepted: 04/08/2025
Available online: 27/12/2025

Abstract

This research study integrates geophysical, satellite remote-sensing, and surface-geology data to derive and enhance the structural and geological understanding of the Busaiya area in southwestern Iraq. An arid climate characterizes this area, which covers 19,500 km^2. Tectonically, the Busaiya area is located in the stable part of the Arabian Platform. In this paper, gravity, magnetic, and seismic reflection data have been investigated to study the surface and subsurface geological structure in more detail, since they could have potential importance in mineral and oil exploration. The interpretation of the gravity and magnetic data shows that the Busaiya is a sub-basin structure located at the southeastern edge of a basement block structure and has been reactivated and subsided throughout geological history. The boundaries and structures of the sub-basin are delineated using edge-detection filters, while depths are determined with the tilt-depth method. Additionally, a two-dimensional depth inversion model, oriented east-northeast and based on gravity data from the northern part of the sub-basin, reveals both lateral and vertical variations in density contrasts. The lineaments revealed by the Global Digital Elevation Model imaging indicate a high density, while the Sentinel-2 data illustrate notable rock deformation along the edges of the sub-basin. The high density of the lineaments could allow the evolution of near-surface, good-quality groundwater aquifers. Regions within the Busaiya sub-basin are recommended for mineral and oil exploration according to their structural situation. It is concluded that the area has undergone significant stress-induced deformation, resulting in subsurface faulting and surface deformation. Moreover, the area has been affected by the anticlockwise movement of the Arabian Plate, which has contributed to a block rotation.

Keywords: Busaiya; structural basin; gravity and magnetic interpretation; block rotation; Iraq

ISSN 1811-4539, EISSN 3005-3714
https://doi.org/10.59150/ibgm2102a13
IBGM: http://ibgm-iq.org/
Academic Scientific Journals: www.iasj.net

1. Introduction

A thick and gently northeast-dipping sedimentary sequence overlies a Precambrian basement in the southwest of Iraq. The Iraq Petroleum Company (IPC) reported a discovery of economically significant oilfields in 1948 in southern Iraq and southwest Iraq in 1960 (Al Naqib, 1967). The southwest area of Iraq covers the southeastern part of a regional basin known as the Widyan Basin, which is regarded as having two total petroleum systems: Paleozoic and Jurassic-total, with estimated oil and petroleum of 62.5 Bbbl (Billion barrels) (Aqrawi, 1998; Fox & Ahlbrandt, 2002). Additionally, some discovered oilfields in southwest Iraq, such as Samawa-1, Abu Khaimah, and Diwan-1, are associated with Cretaceous limestone.

Southwestern Iraq has primarily been explored through regional surface and subsurface geological studies, as evidenced by research conducted by Al-Hashimi (1973), Al-Mubarak & Amin (1983), Al Naqib (1967), Buday (1980), and Tamar-Agha & Al-Sagri (2015). These studies have provided foundational insights into the area's geological features but remain limited in scope. The discovery of subsurface geology in the southwestern region of Iraq has largely relied on regional data, including gravity, aeromagnetic, and borehole data, as noted by Jassim & Buday (2006) and Tamar-Agha & Al-Sagri (2015). This suggests that further studies, including local surface and subsurface geology, are needed to discover new energy and mineral resources in the southwestern part of Iraq. The study area (defined here as the Busaiya area) covers approximately 19,500 km^2, containing the town of Busaiya, and lies southeast of the stable Platform of Iraq (Figure 1). The most noticeable thing in the Busaiya area is the surface geology that displays a distinctive sequence of middle Miocene carbonates and evaporated rocks to Quaternary sediments. Recently, Al-Bahadily et al. (2024) used aeromagnetic data to interpret the geological structures of the basement beneath this part of Iraq. They showed that the Busaiya area is bounded by a north-south-trending graben at an estimated depth of about 9 km.

Several international and local studies that integrate geophysical methods with surface geology data to study the structural and tectonic settings at different scales (e.g., Acton et al., 1991; Bonhommet et al., 1988; DeMets et al., 2010; Horst et al., 2018; Jackson & Molnar, 1990; McCaffrey et al., 2000; Numan & Bakose, 1997). This study aims to improve the subsurface geological knowledge of the Busaiya area by integrating gravity, aeromagnetic, 2D seismic reflection, Global Digital Elevation Model (GDEM) downloaded from the website http:// gdemdl.aster.jspacesystems.or.jp/index_en.html, Sentinel-2 high-resolution images, available at https://www.satimagingcorp.com/satellite-sensors/other-satellite-sensors/sentinel-2a/, and surface geological data. The products of this work are of help in different geological explorations, including hydrocarbon, mineral, and groundwater resources. It also aids the interpretation of some surface geological features that have remained for a long time of unknown origin. Potential field data has been widely used to study the structural framework and delineate the subsurface geological structures (recent examples are Al-Bahadily Al-Rahim et al. (2024), Alvandi Su et al. (2023), Alvandi, Toktay et al. (2023), Ekwok et al.

2023, Long et al. (2025), Pham et al. (2025), Pham & Eldosouky (2025), Qadir et al. (2023), and Wang et al. (2022). However, satellite images can be used to indicate surface lineaments, the neotectonic activity, and reactivated linear structures that are controlled by subsurface sources. To achieve the goal of this study, we first processed the gravity and magnetic data to reveal the geological structures within the sedimentary cover and basement rocks, respectively. Then, depths to the tops of these structures are estimated using 1D power spectrum analysis and tilt depth methods. After that, the satellite images are studied and analyzed to derive the dominant lineament trend in the Busaiya area. Finally, conclusions are drawn based on the interpreted surface and subsurface data.

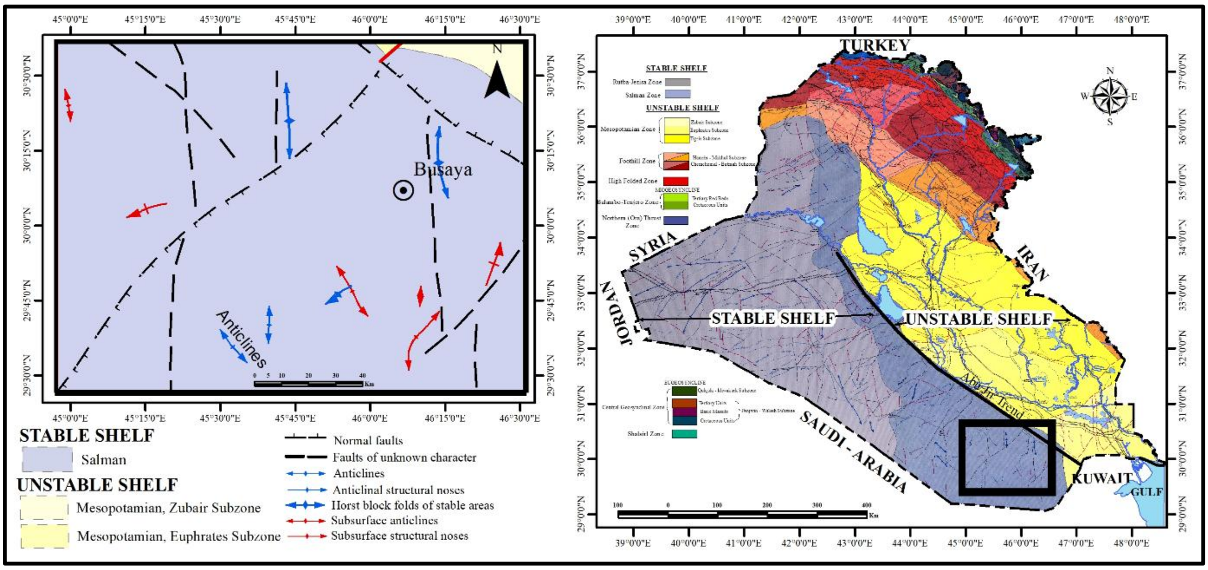

Figure 1. A) The tectonic map of Iraq shows the location of the Busaiya area within the Stable Shelf, Salman zone (black box) (modified after Buday & Jassim, 1984). B) A zoomed view of the black box in the tectonic map demonstrates the structural elements in the Busaiya area. Note that the structural elements have different orientations.

2. Geological and structural setting

The Busaiya area is a physiographic region within the Iraqi desert and is characterized by an arid climate. The Busaiya area is tectonically located in the stable shelf zone of the northeastern Arabian Platform (Figure 1A). The tectonic boundary separating the stable and unstable shelf is represented by the northwest (NW)-southeast (SE)-trending Abu Jir Fault System that is located just to the east (E) and northeast (NE) of the Busaiya area (Figure 1A). The surface geology consists of sedimentary rocks and sediments ranging in age from the Middle Eocene to the Quaternary. The structural elements map (Figure 1B) shows folds that are related to an unknown source, according to Jassim & Buday (2006b). The central part displays a distinctive local succession of middle and Late Eocene shallow marine limestone (Dammam Formation) to the Miocene Formations (composed of carbonate, evaporated, and clastic facies) (Figure 2). The Dammam Formation is highly karstified, and some karst depressions are filled with Pliocene-Pleistocene clastic-limestone sediments (Zahra

Formation). The surface depressions are filled with the Zahra Formation and recent sediments that align in NW and NNW directions and are mostly connected with the enhancement of inherited basement weak zones, such as the Najd Fault System [approximately 670 million years ago (Ma)]. This succession is uncomfortably bound from the south and southwest by Pliocene-Pleistocene clastic sediments of the Dibdibba Formation, and the boundary is represented by a NE – SW structural cliff that is a steep and SW-trending cliff of six meters high (Al-Ani & Ma'ala, 1983) (Figure 2). The present surface of the Busaiya area is affected by the latest (second) compression phase of the Alpine Orogeny, which started in the late Miocene-Pliocene and created plateaus with a gentle slope towards NE (Ma'ala, 2009a). Seasonal rivers pass from the SW to the NE parallel to the structural cliffs and some surface lineaments. Evidence of neotectonic activity is recorded in southern and southwestern Iraq. Such evidence includes influencing the environments of sedimentation (Al Naqib, 1967), the major surface lineament system of NE – SW direction acts as an abrupt limit for Miocene-Pleistocene formations (Al-Amiri, 1979; Al-Hashimi, 1973; Ma'ala, 2009b; Sissakian & Deikran, 1998), sudden changes in the major valley courses (Al-Gurairy, 2023), and surface subsidence due to reactivation of normal faults reaching the surface (Al-Bahadily, Al-Rahim, et al., 2024a).

Reactivation of horsts and grabens structures that developed during the extensional phase in the Carboniferous (Hercynian Orogeny) and structural noses and short anticlines that formed along transversal faults within the basement act as hydrocarbon traps (Fox & Ahlbrandt, 2002; S. Jassim & Buday, 2006b). Basement depth in the Busaiya area ranges from approximately 4.5 km in the northern part to 9 km in the southern part (Al-Bahadily & Al-Rahim, 2024). According to Al-Bahadily, Fairhead et al. (2024), these variations in basement depth are related to the influence of basement blocks and graben structures. The main structural elements of the Busaiya area are illustrated in Figure 1B.

3. Data used and methodology

The following data sources are used.

- The potential field data set is represented by gravity and magnetic data covering the entire Busaiya area. The gravity data are presented as a complete Bouguer anomaly (CBA), while total magnetic intensity data have been transformed to reduced-to-pole (RTP). The cell size of the gravity grid file is 1000 m, while the RTP grid file is 520 m. The gravity map (Figure 3a) reveals a significant low beneath the Busaiya area that may indicate a sub-basin structure within the sedimentary overburden. The RTP map (Figure 3b) highlights a basement low, suggesting the existence of a deep sub-basin.

A 2D seismic reflection survey in the Busaiya-Ubaid area (Bu) was carried out by the Sixth Crew, Iraq National Oil Company (INOC6) from 1984 to 1987. This survey was conducted using Vibroseis sources to delineate geological structures and search for possible oil traps, including structural and stratigraphic traps. Three processed seismic lines from this survey used in this study are **Ba-17**, **Bu-42**, and **WI-24**. Unfortunately, the quality of the seismic data ranges from poor to intermediate due to the acoustic nature of the sediments.

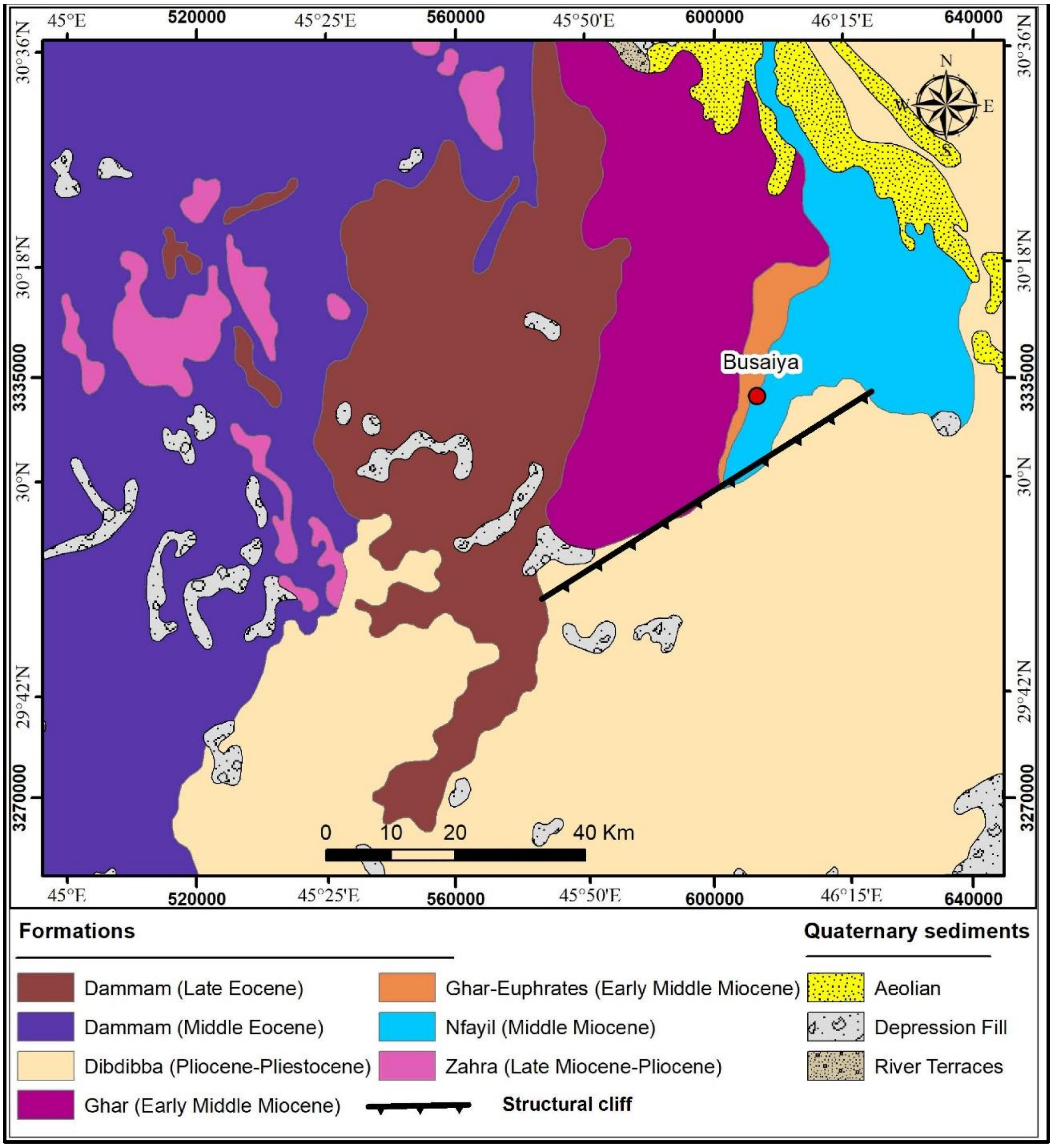

Figure 2. Geological map of the Busaiya area (study area) (modified from Sissakian & Fouad, 2012) showing the middle Eocene (Dammam limestone Formation) to Pliocene-Pleistocene (Dibdibba Formation) successions in the E – W direction. Note the extensions of aeolian sand and the surface depressions filled with Zahra Formation and Recent sediments that align in NW and NNW directions, mostly connected with the enhancement of inherited basement weak zones that coincided with the Najd Fault System (approximately 670 Ma).

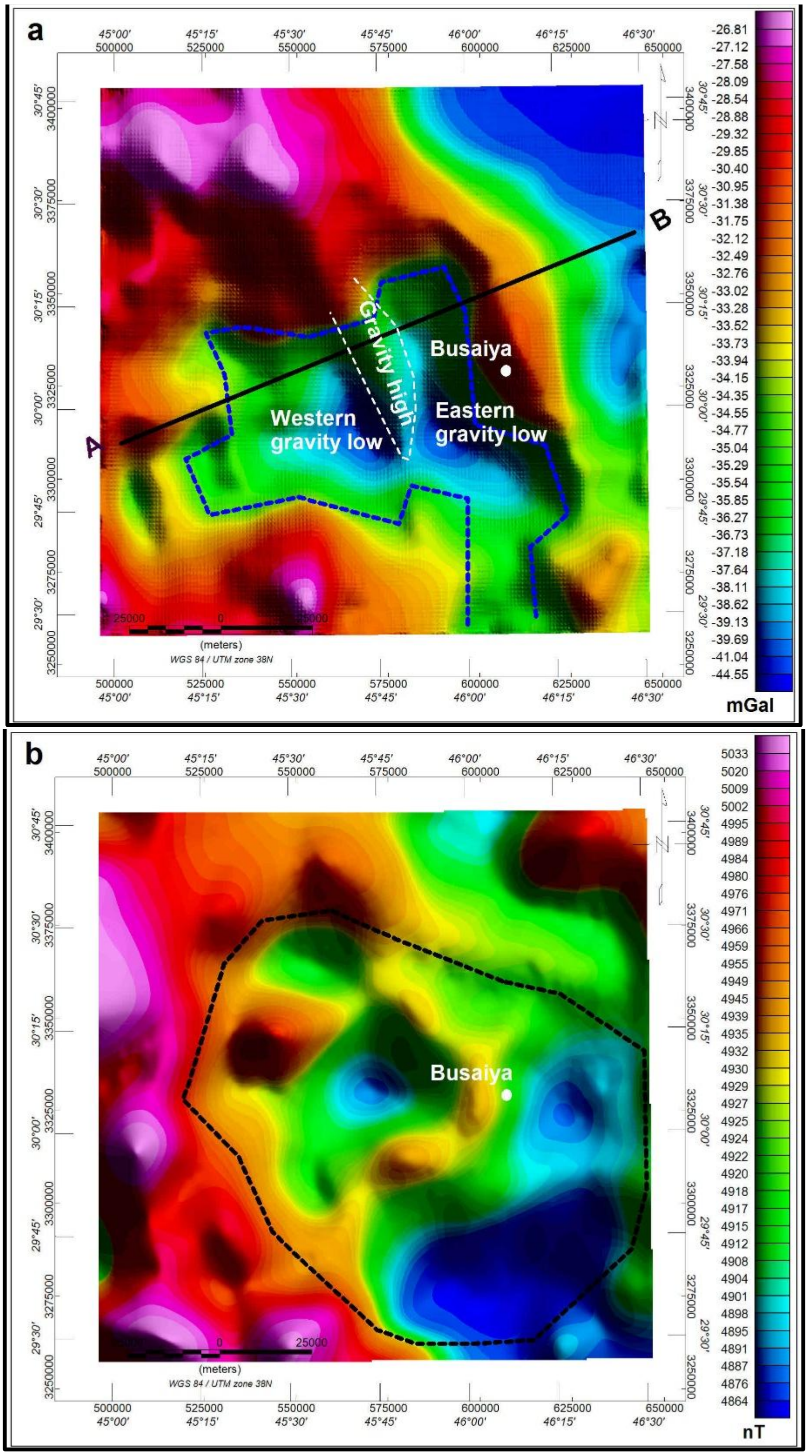

Figure 3. Gravity and magnetic field data of the Busaiya area. (a) Complete Bouguer anomaly map. Note the gravity low (blue dashed line) west of the Busaiya, and it is divided into two lows: eastern and western by a gravity high. (b) Reduced-to-pole (RTP) map. Note the RTP lows on both sides of the Busaiya and to the extreme south (black dashed line). Both the gravity- and magnetic-derived basins are deduced from the present study.

- The satellite data, Sentinel-2, and the Advanced Spaceborne Thermal Emission and Reflection Radiometer Global Digital Elevation Model (ASTER GDEM), are used to automatically extract lineaments. Two reasons for this investigation were the difficulty of ground access to certain sites and the large geographical extent of the Busaiya area.

Faults in the seismic sections were **identified depending on reflector discontinuity, vertical/inclined shifts,** termination of layers, and r**epetition/omission** sequences. The results obtained from the gravity method are compared with the results of the magnetic method and then integrated with seismic data, surface geology, and surface lineaments derived from satellite images to reveal the final interpretation.

4. Data processing

Gravity data processing involves several steps, including removing high-frequency content, gravity field analysis using the power spectrum method, edge-detection of gravity sources, estimating depth-to-tops of gravity sources, and density-depth inversion along a 2D profile. We applied the modified non-local means approach to gravity data to eliminate high-frequency content, including noise.

The edges of gravity sources are delineated by applying the modified horizontal gradient amplitude (MHGA) filter (Ai, Deniz Toktay, et al., 2024) and the total horizontal gradient (THG) filter (Cordell, 1979).

The THG is defined as:

$$\sqrt{\left(\frac{\partial f}{\partial x}\right)^2+\left(\frac{\partial f}{\partial y}\right)^2} \tag{1}$$

Where $\frac{\partial f}{\partial x}$ and $\frac{\partial f}{\partial y}$ are the 1st-order derivatives of the gravity/magnetic field ($\boldsymbol{f}$) in the $\boldsymbol{x}$ and $\boldsymbol{y}$ directions, respectively.

:The MHGA is expressed as

$$\text{MHGA} = \frac{|R+1|\text{-}|R\text{-}1|}{2} \tag{2}$$

Where

$$R=\left(\frac{\frac{\partial THG}{\partial z}}{\sqrt{\left(\frac{\partial THG}{\partial x}\right)^2+\left(\frac{\partial THG}{\partial y}\right)^2}}-\frac{\pi}{3}\right) \tag{3}$$

The amplitude of the MHGA is between -1 and 1, and the amplitude maxima are located at the edges of the causative sources.

The 2D classical compact inversion is applied to gravity data along an ENE profile, which is approximately parallel to the available seismic sections (as discussed in the next section). A comprehensive and detailed description of the compact inversion technique that utilizes a mixed weighting function can be found in the work by Ai, Essa, et al. (2024). This resource thoroughly explores the methodology, applications, and implications of the approach.

Depth to the tops of gravity lineaments is estimated using the tilt-depth method (Salem et al., 2007), and the depth to the top of gravity sources is estimated using the 1D power spectrum technique proposed by Spector & Grant (1970). The boundaries of the sub-basin structure within the sedimentary cover are determined based on the boundaries of the gravity low shown in the residual gravity map (Figure 3a), which was determined based on the fault lineaments derived from edge-detection filters.

Also, analyzing the RTP grid using a 1D power spectrum approach produced three distinct depth slices: deep, intermediate, and shallow sources corresponding to deep basement sources, shallow basement sources (structures), and noise, respectively. The edges of both deep and shallow basement sources were delineated by implementing the THG filter. The boundaries of the sub-basin structure within the basement were determined based on the results of the edge filter, which defines the RTP magnetic low.

However, conventional surface lineament mapping methods are inefficient in identifying all existing lineaments and their extensions effectively. Therefore, we performed automatic lineament extraction using ASTER-GDEM data. The GDEM provides topographic and hydrological information such as elevation, slope, and streams at a spatial resolution of 30 meters. Aster GDEM and Sentinel-2 data were projected into the UTM (Universal Transverse Mercator Projection) coordinate system in zone 38-North, which coincides with the geographic position of the Busaiya area.

There is no single technique for geological lineament detection in remote sensing; instead, lineaments are typically extracted using one of three methods: manual, semi-automated, and automated. Satellite images from Sentinel-2 and Aster GDEM were processed using Erdas Imagine 2022, PCI Geomatica 2016, and GIS to identify geological features and map the distribution and density of lineaments in the Busaiya area. Additionally, Rockwork 16 was used to produce a rose diagram. The integration of Sentinel-2 remote sensing data and ASTER DEM data provides highly valuable information for geological interpretation. Surface lineament analysis is an essential tool in geological mapping and mineral exploration. In this study, surface lineaments are extracted using an automated technique known for its efficiency, simplicity, speed, and high reproducibility. However, before extracting lineaments from remote sensing data, pre-processing of the ASTER GDEM is necessary. The LINE module algorithm in the PCI Geomatica 2016 is used for automatic extraction of lineaments from images.

5. Results

5.1. Gravity method

The results of applying the MHGA filter to the Bouguer anomaly grid are presented in Figure 4, and the outputs of the THG filter are superimposed on this figure as white lines for comparison. The comparison shows that all the MHGA maxima align with the THG-derived lineaments, confirming the existence of these lineaments through two techniques. The boundaries of the gravity low shown in Figure 3a, interpreted as a sub-basin structure, are determined based on the MHGA- and THG-derived lineaments and are represented by a black dashed line in Figure 4. The sub-basin is divided into two distinct lows, eastern and western, by an NNW – SSE-trending gravity high (Figure 3a), which is also detected by both edge filters. Moreover, power spectrum analysis estimates the depths as follows: 12,600 m for the deep sources of the Busaiya sub-basin, 3,780 m for the western low, 5,380 m for the eastern low, and 2,230 m for the NNW – SSE-trending gravity high.

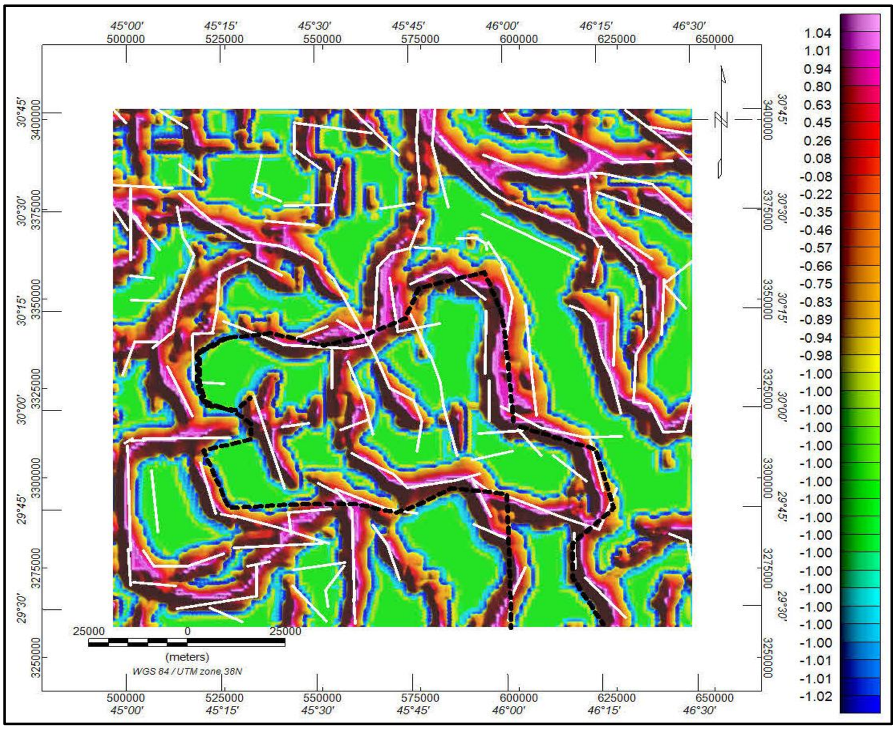

Figure 4. Products of implementing the MHGA (the base map) and THG filters (posted as a straight white line) on the Bouguer grid. Both filters display the same edges of the gravity sources; the bold dashed black line indicates the interpreted Busaiya sub-basin.

The tilt-depth method has been applied to the MHGA-derived lineaments to estimate the depth-to-top of these lineaments, and the results are shown in Figure 5. The estimated depths range from deep, up to 12,000 m, and shallow near the ground surface. The deep estimations

(12,000 m) agree with the deep source of the Busaiya sub-basin obtained from 1D power spectrum depth estimates (12,600 m).

Figure (6a) displays the azimuth rose diagram of gravity-derived lineaments, revealing two dominant trends: a NE – SW direction and a NW – SE direction. The majority of these lineaments are located at depths less than 5,000 m (as indicated by the blue color in Figure 6a). This is also shown by the histogram analysis, where these lineaments have an average depth of 2,000 m (Figure 6b). Such depths lie within sedimentary cover.

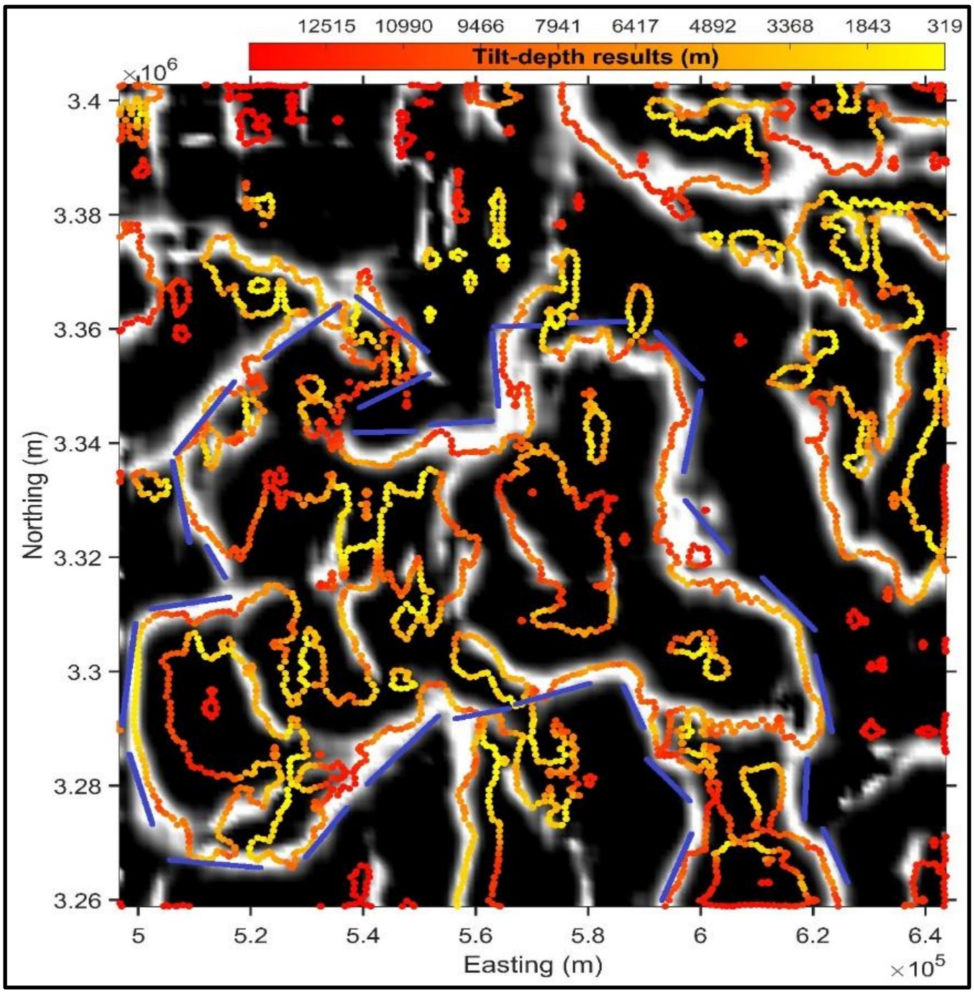

Figure 5. Depth estimates obtained from the tilt-depth method for the edges detected by the MHGA filter (see text for more explanation). Some edges have high estimated depths (10,000 to 12,000 m, appear in red), while others have shallow estimated depths of less than 1,000 m (appear in light orange and yellow). Edges characterized by nearly the same color refer to normal fault lineaments (sub-basin boundaries), whereas edges characterized by variable depths may indicate fault traces at different depth levels. The blue dashed line indicates the sub-basin boundaries derived from gravity data.

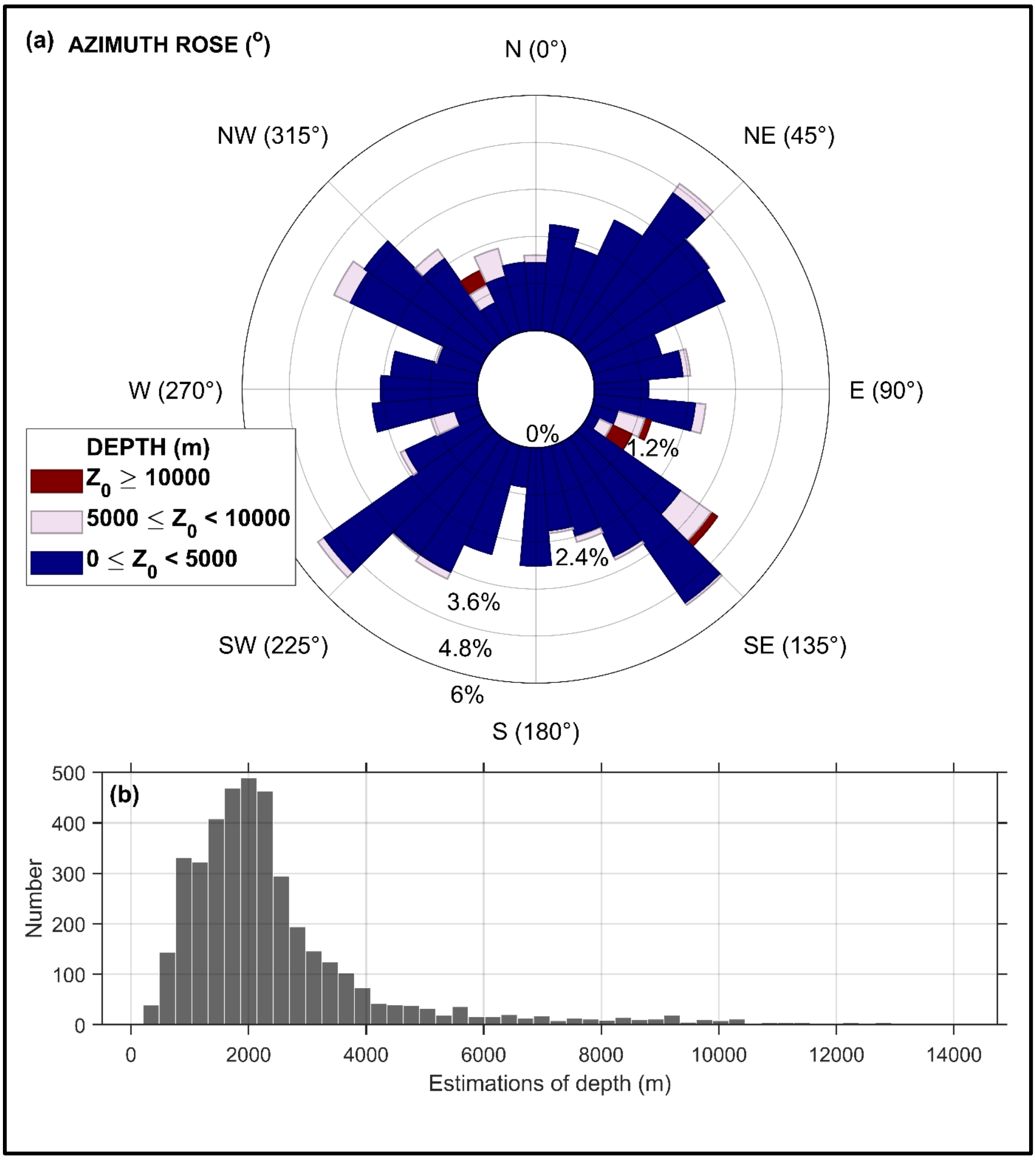

Figure 6. Lineament analysis of gravity data. (a) Azimuth rose diagram showing two dominant lineament directions: NE – SW and NW – SE. (b) A histogram of the analyzed lineaments shows that the majority have an estimated depth of 2,000 m based on the results of the tilt-depth method.

The results of density-depth inversion along an ENE-trending gravity profile AB (its location appears in Figure 3a) are presented in Figure 7. The length of this profile is about 140 km, and it is parallel to the general trend of the seismic sections. Figure 7 shows the inversion results obtained via compact inversion. The inversion parameters of compact inversion are set as *Max_iter*=10, μ=0.1, ζ=2, ξ=0.9, and $\varepsilon=10^{-4}$. Refer to Ai, Essa et al. (2024) for the definition of these parameters. Figure 7a exhibits the optimum successful data-fitting performance of the compact inversion technique. Figure 7b illustrates the reconstructed subsurface structures using the compact inversion. The sub-basin structure is satisfactorily shown.

Correspondingly, Figures 7c – e show the variation behaviors of the three stopping criteria against iterations.

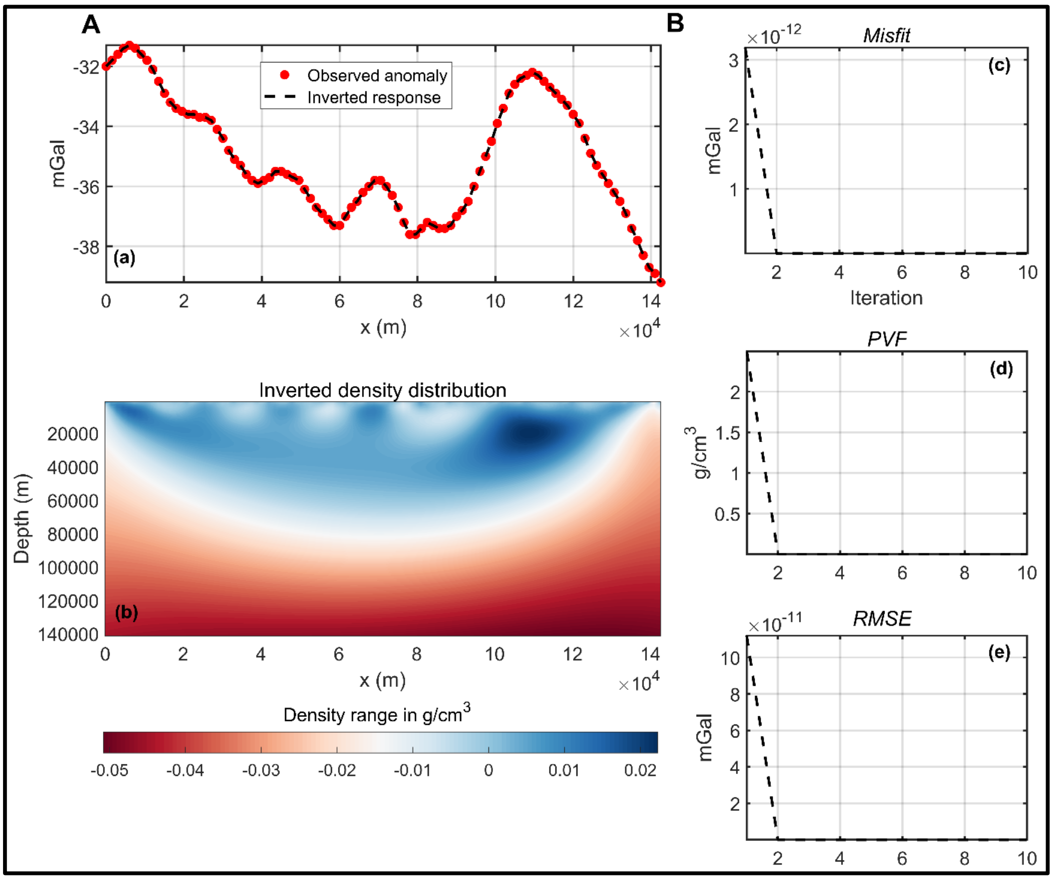

Figure 7. Density-depth inversion along the gravity profile AB, its location appears in Figure 3a. (a) The fitting performance of compact inversion, (b) demonstrates the density distribution of the subsurface obtained via compact inversion, (c)-(e) shows the variation behavior of three criteria against iterations.

5.2. Magnetic method

By applying the technique suggested by Spector & Grant (1970) to the RTP grid, the power spectrum plot displays three distinctive straight lines (not presented), corresponding to low, intermediate, and high frequencies. These represent deep, intermediate, and shallow sources. The high-frequency content includes shallow and low-amplitude magnetic anomalies associated with faults in sedimentary cover (Al-Bahadily, Fairhead, et al., 2024). These are treated as noise and can be excluded by subtracting them from the original RTP grid. This filtering technique aids in performing magnetic field separation (Cowan & Cowan, 1993), obtaining three depth slices accordingly. The average estimated depths for the deep, intermediate, and shallow magnetic sources are 11,600 m, 4,910 m, and 1,450 m (noise). Figure (8a and b) displays the depth slices of the deep and intermediate basement sources.

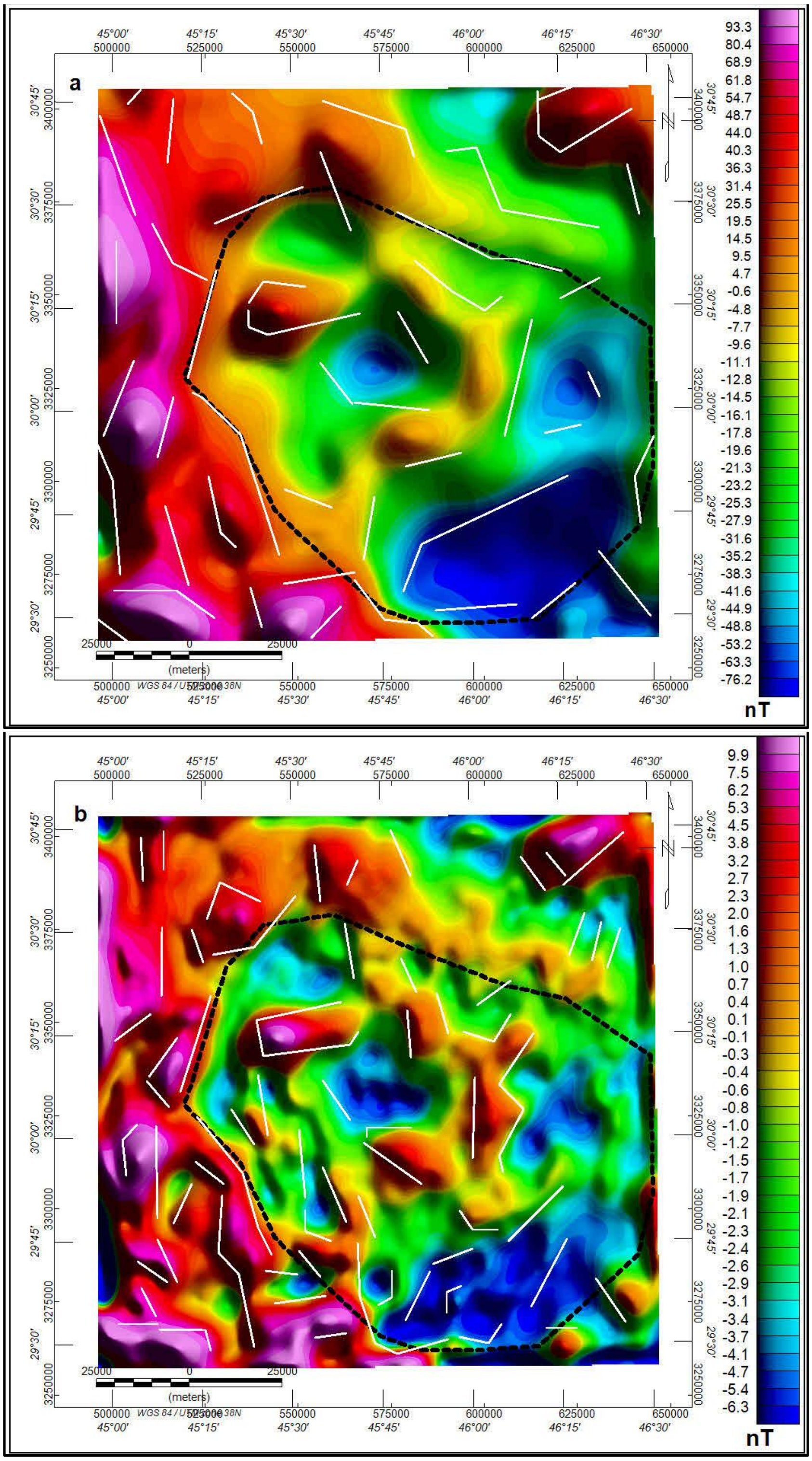

Figure 8. Magnetic sources of the RTP map obtained from 1D power spectrum analysis. (a) Deep basement sources from a depth slice of 11,600 m and (b) shallow basement sources from a depth slice of 4,910 m. White straight lines represent a high magnetic gradient derived from the THG filter. The black dashed polygon highlights the Busaiya sub-basin boundaries, which are drawn based on the magnetic low (Figure 3b) and high gradient lineaments (faults) derived from the THG filter.

The THG filter has been applied to the grids shown in Figure 8a and b, and the THG-derived lineaments are posted on the figure as white straight lines. The THG filter outlines the regions of high-gradient fields, which are mostly related to fault systems. The dominant lineament trends are NE – SW and N – S (Figure 8a). An NW – SE-trending lineament is observed in the central part of the Busaiya area. This trend coincided with the basement-inherited Najd Fault System (670 Ma). The interpreted Busaiya sub-basin boundary is outlined based on fault lineaments derived from the THG filter and posted in Figure 8a as a dotted black line. The depth-to-basement in the Busaiya area ranges between 4.5 km and 9.5 km, according to the depth map prepared by Al-Bahadily & Al-Rahim, 2024. They reported that the basement in the northeast of the Busaiya area (north Busaiya town Figure 9 is ~ 4.5 km deep and is mostly the shallowest basement recorded in Iraqi territory. This basement high has an arcuate shape, and the surrounding basement low is up to 9.5 km deep in the southeastern part of the Busaiya area (Figure 9).

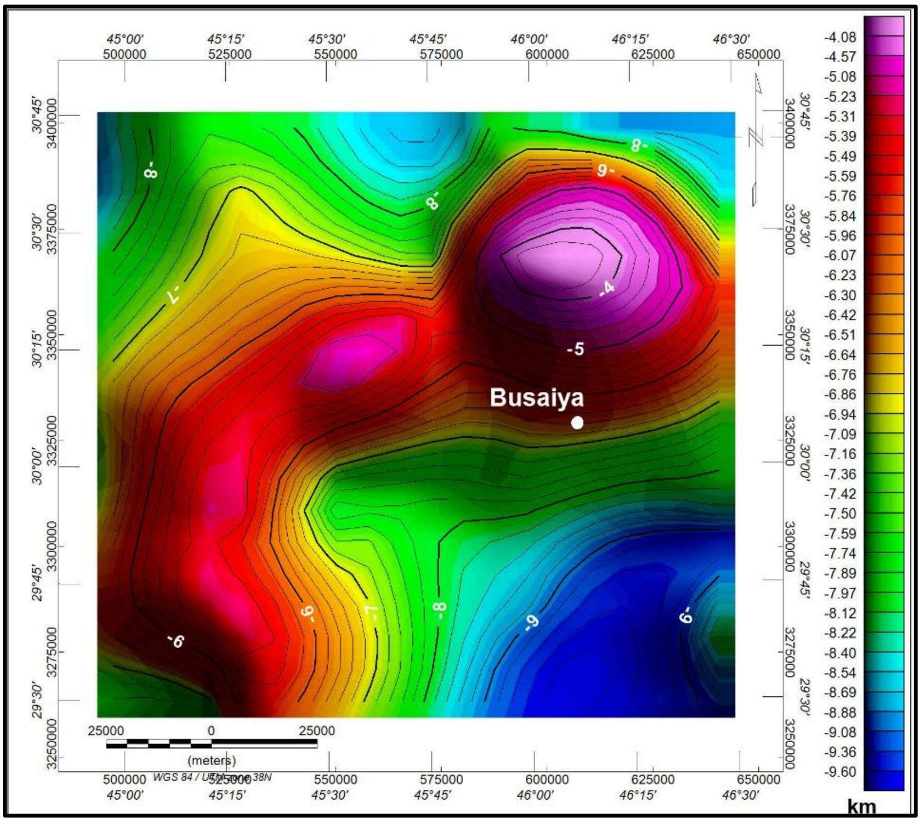

Figure 9. The basement surface map beneath the Busaiya area displays a curved or arcuate basement high of ~4.5 km deep and a basement low of ~ 9.5 km deep in the southeastern part.

5.3. Seismic sections

The current interpretation of the seismic sections indicates a general dipping of the geological layers from the west towards the east (Figure 10, upper panel). Additionally, the analysis reveals that the area is affected by systems of normal faults resulting from a regional extension (Figure 10, upper panel). Three 2D seismic sections, **Ba-17**, **Bu-42**, and **WI-24**, traverse the upper central part of the Busaiya area in NE-SW and ENE-WSW directions

(Figure 10). The seismic sections, along with the interpreted Busaiya sub-basin structure and the THG fault/lineament structures, are superimposed on the Bouguer gravity map to show the relationship between them. The **Bu-42** seismic section overlays an NNW – SSE gravity high that separates the main gravity low (Busaiya sub-basin) into two gravity lows. This section also passes through the eastern edge of the sub-basin, cutting many faults (straight white lines) that indicate the poor quality of this section. The other two sections exhibit intermediate quality and contain numerous faults of different extensions and offsets. These faults align with the lineaments (faults) deduced from the THG filter, which are intersected by these sections (see the gravity map shown in the lower panel of Figure 10). Gravity-derived lineaments that coincide with interpreted seismic faults were numbered 1-4 in the gravity map and the seismic sections for comparison (Figure 10).

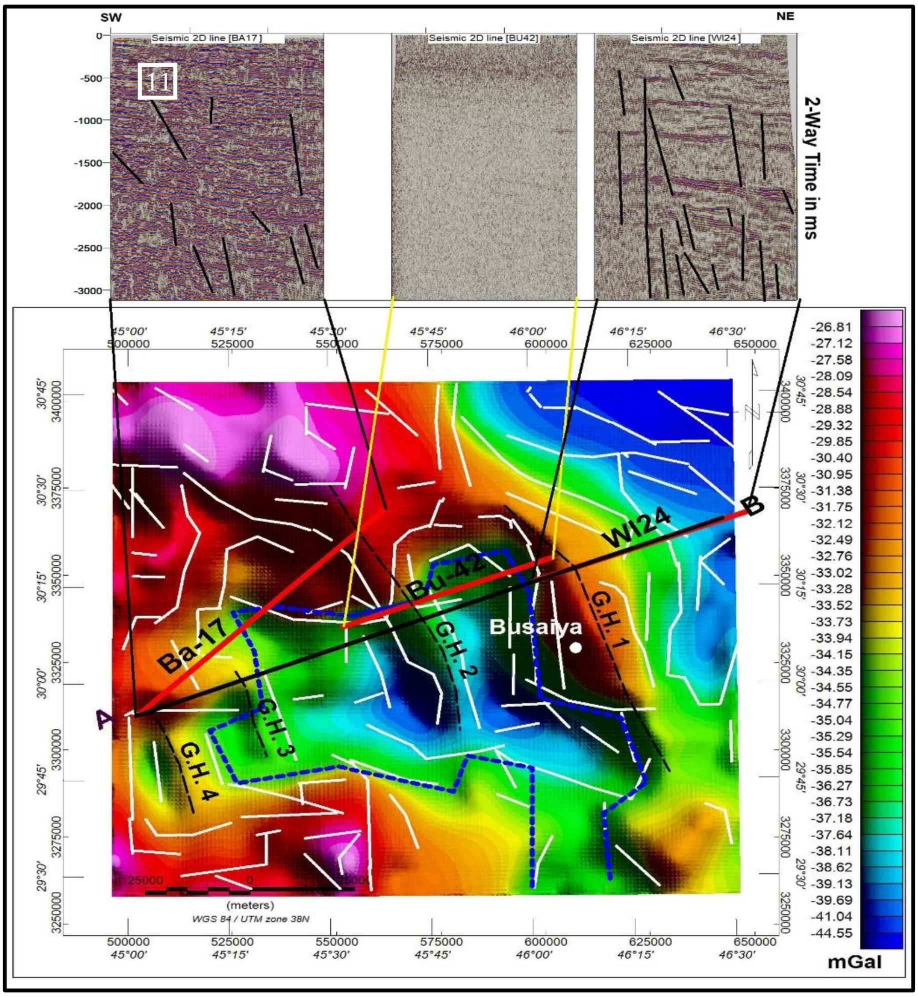

Figure 10. Interpreted gravity map (lower panel). The white straight lines are lineaments/ faults derived from the THG filter. The blue dashed line represents the interpreted Busaiya sub-basin boundaries, which are drawn based on the THG faults and the gravity lows. **Ba-17**, **Bu-24**, and **WI-24** are 2D seismic sections with their interpretation being displayed in the upper panel for comparison with gravity lineaments and anomalies. The profile AB is a 2D density-depth section used in Figure 7. The approximate depth of the 2D seismic sections Ba-17 and WI-24 is 7500 m, calculated at an average velocity of 2500 m/sec.

5.4. Satellite images

The upper panel of Figure (11) presents Sentinel-2 satellite imagery of the Busaiya area, revealing surface deformation, near the edges of the sub-basin (white line), characterized by folding and undulations in the outcrops of Eocene formations, which can be observed when zooming, for example, regions inside the black boxes, in the lower panel of Figure (11). This deformation indicates that the area has been subjected to compressional stresses. Further, the surface lineament density map derived from this imagery shows that the highest lineament density delineates the deformation regions (Figure 12a). Based on the derived lineaments, there are two dominant trends: an NNW – SSE major trend and an ESE – WNW minor trend (Figure 12b). However, the drainage network of the Busaiya area displays stream orders from the first to the fifth (Figure 12c). The fourth and fifth stream orders show three distinctive directions: NE, NS, and NNW, which are affected by the surface deformation shown in Figure 11, indicating neotectonic activity. Based on the slope classification map of the Busaiya area, most of the area is dominated by semi-flat to very gentle slopes, while the medium and steep to very steep slopes cover very limited areas, as shown in Figure 12d. Although the general trend of the drainage pattern is with a general gradient from southwest to northeast, there is a local change in the area toward the northwest, primarily due to topographic influence.

6. Discussion

This study demonstrates the integration of geophysical and remote sensing data to enhance surface and subsurface geologic knowledge in the Busaiya area. Various data sources, including geological, geophysical, and remotely sensed imagery, have been used to determine the distribution and depth information of surface and subsurface geological structures. The visual interpretation of the Sentinel-2 images and the extracted lineaments from GDEM revealed a strong similarity in concentration and orientation of lineament with visible deformation and folding surrounding the sub-basin boundaries, as shown in Figures 11 and 12. Lineaments show N – S main direction as well as the WNW–ESW direction (Figure 12b). In addition, the neotectonic activity can be studied by analyzing satellite and GDEM images (recent examples: Taib et al., 2024; Valkanou et al., 2021). Besides the evidence of the neotectonic activity in the Busaiya area that is submitted in **Section 2**, we add another clue of neotectonic activity in the area. The drainage network of the fourth- and fifth-order streams (Figure 12c) displays different orientations, including NE, N – S, and NNW directions, coinciding with the surface deformation and the dominant fracturing orientations in the area (Figures 11 and 12). The basin boundary derived from gravity data is posted on Figures 11 and 12 for comparison.

Lineament analysis, both at the surface and sub-surface, plays a crucial role in exploration geophysics. Aster GDEM-derived lineaments offer an idea about fracture density that helps define fresh groundwater resources in arid and semi-arid regions. Surface lineaments also help in determining geological structures influenced by various stress sources, including dominant tectonic stress fields and neotectonic activities. Additionally, these lineaments can reveal connections to deeper geological structures. Gravity data-derived lineaments, however, are essential in hydrocarbon exploration and aid in seismic reflection interpretation (S. Shevchenko, 2017; S. I. Shevchenko & Iasky, 2004). Fault lineaments act as structural traps and delineate basin/sub-basin boundaries. The depths of the gravity-derived lineaments estimated using the tilt-depth method (Figure 5) agree with the estimated depths of gravity anomalies using the 1D power spectrum plots. However, the tilt-depth method supposes that the lineaments (contacts/faults) must be vertical or nearly vertical (Salem et al., 2007); otherwise, the estimated depths may not be accurate. However, magnetic-derived lineaments contribute to studying deep basement structures and basin and block boundaries, which are linked to dominant structural and tectonic stresses and regions of reactivated faults.

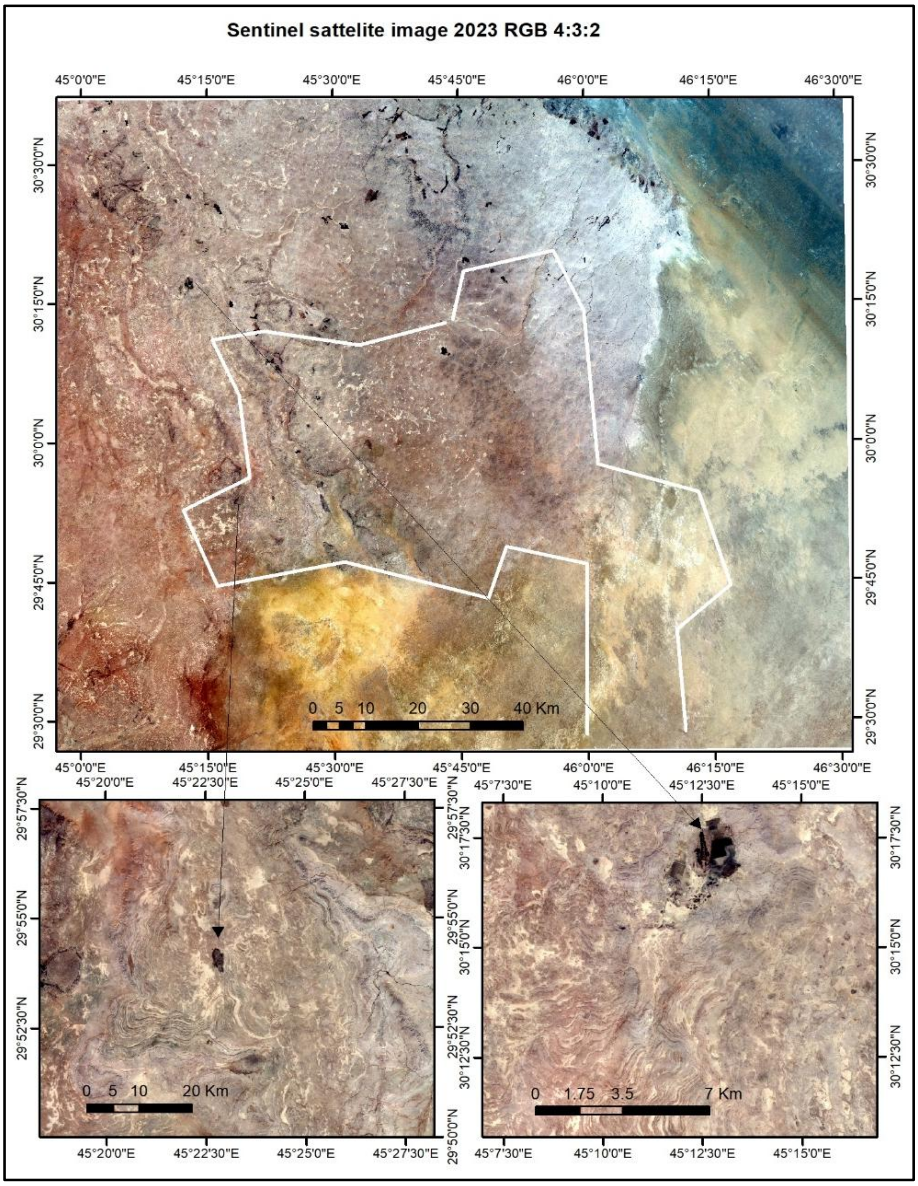

Figure 11. Sentinel-2 satellite image of the Busaiya area (upper panel) used in studying the main surface features and lineaments. Surface deformations are easily seen when zooming in on the image, like the regions outlined by black boxes in the lower panel. The white line indicates the boundary of the basin derived from gravity data.

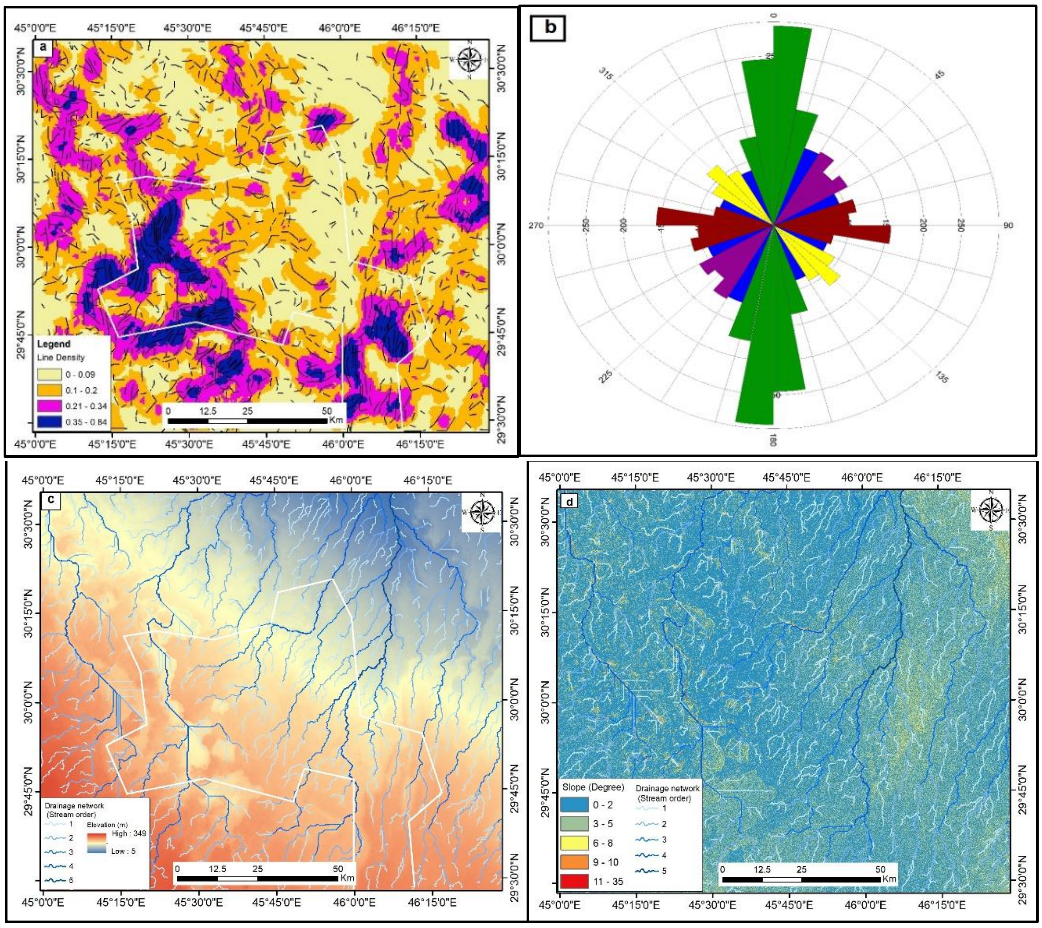

Figure 12. Analysis of satellite images of the Busaiya area. (a) Surface lineament density map. Note the high lineament density, consistency with the surface geology that outlines the sub-basin. (b) The rose azimuth diagram for the surface lineaments displays two dominant trends. (c) The drainage network map displays stream orders. (d) Slope classification map. The bold white line is indicated in Figure 11.

The present study identifies three distinct sub-basin boundaries: the first revealed from the significant variations in surface geology, and the other two are derived from gravity and magnetic data. An east-west-trending geological succession of Miocene sequences, which can also be seen in the lineament's density map (see regions of high lineament density in Figure 12a) and the boundaries of gravity and magnetic lows deduced from edge-detection filters (respectively, blue and black dashed lines in Figures 8 and 10. Although these sub-basin boundaries have different shapes and extents, they generally overlap. The relative differences in sub-basin shape and boundaries are expected since these boundaries are drawn based on different physical properties. The initial sub-basin, which corresponds to the basement-related structures, is defined by faults that may change their trajectories through the sedimentary cover and ground surface during reactivation periods. Additionally, boundaries identified through magnetic data, based on contrasts in magnetic susceptibility, differ from those derived from gravity data, which rely on density contrasts. Both, in turn, differ from the physical boundaries observed in surface geology, which are influenced by various factors, including topography, paleogeography, and erosion.

Figure 9 depicts an arcuate basement high of 4.5 km deep (nominated as the north Busaiya high), bound by a basement low (Busaiya sub-basin) from the southeast. This structural condition may indicate rotation to accommodate compressional stress from the counterclockwise movement of the Arabian Plate. We propose that since the late Miocene, the complex stress field in the Busaiya area has reactivated basement faults, leading to the arcuate structure and the Busaiya sub-basin shown in Figure 9.

Another example of a complex stress field observed in the magnetic map is the en echelon fault structures oriented in the N-S direction, in the central northeastern part (Figure 8b), which indicate non-coaxial shear stresses. Such structural arrangements of en echelon magnetic anomalies have been linked to transtensional tectonics and provide insights into the region's tectonic evolution (e.g., Bracey, 1968; Le Pichon & Heirtzler, 1968; Wagner, 1987; Yamazaki & Yuasa, 1998), and may have economic value in hydrocarbon potential (Leyla et al., 2015), geothermal studies (Zaal et al., 2021), and mineral exploration (Johnston et al., 1996). Furthermore, the visual evidence of surface deformation and folding, along with the previously mentioned three directional patterns of fourth- and fifth-order drainage streams, suggests rotational movement. These streams exhibit an anticlockwise progression, transitioning from NE to NS and then to NNW (Figure 12c). The observed surface deformation and folding, likely associated with block rotation and neotectonic activity, may provide insight into the previously unclear origins of the folds in the southern Salman Zone, including the Busaiya area (Figure 1B), as noted by Jassim & Buday, 2006b.

In the gravity map, much evidence shows that the Busaiya sub-basin lies in a region of a complex stress field resulting from the ongoing Alpine Orogeny. Four parallel gravity highs (indicated by thin dashed black lines numbered G.H. 1 to G.H. 4, Figure 10) are identified in the Busaiya area. These features, interpreted as structural highs, exhibit a decrease in structural amplitude with increasing distance from the Arabian-Eurasian Plate collision zone, located at the far eastern Iraqi-Iranian borders (Figure 1). The first high, which has the largest amplitude, marks the eastern boundary of the sub-basin. The second high divides the Busaiya sub-basin into two parts: the eastern part (the larger) and the western part (Figure 3a). The third and fourth highs subdivide the western part of the Busaiya sub-basin into two structural lows (Figure 10). The third one of relatively lower amplitude seems to be the younger feature. These structural uplifts may have significance in petroleum exploration as they act as structural traps. The NW-trending lineament system is an inherited basement weak zone, well-known as the Najd Fault System, that dominated Arabia in 670 Ma. (Fox & Ahlbrandt, 2002; S. Z. Jassim, 2006).

It is possible that the Ediacaran–late Neoproterozoic Hormuz salt could cause surface deformations in southern Iraq due to salt tectonics. This occurrence, however, has only been observed in one location, Jabal Sanam, which is located about 80 km east of the Busaiya area in the extreme south of Iraq (see, for example, Smith, 2012). Jabal Sanam is a salt plug and dome-like structure similar to those that exist in southwestern Iran and the Gulf (Soltan, 2020). From a structural perspective, Jabal Sanam differs significantly from the Busaiya sub-basin. Moreover, the surface and subsurface evidence presented in this study suggests that a block rotation is responsible for the formation of these structures.

7. Conclusions

The integrated analysis of gravity, magnetic, seismic reflection, surface geology, and satellite remote sensing data of the Busaiya area, southwest Iraq, reveals that the area has a particular tectonic and structural position. Magnetic interpretation indicates that the area represents a sub-basin located at the margin of a basement block and bounded to the south by a basement graben. The northern part features an arcuate structure identified as a basement high and is considered the shallowest basement within Iraqi territory, with an estimated depth of approximately 4.5 km. The fault structures, delineated by edge-detection filters, may act as structural traps for hydrocarbon accumulation. Surface deformation can be readily seen throughout the study area, indicating the impact of compressional stresses and neotectonic activity. This deformation is associated with high lineament density on the surface, mostly in N-S and WSW-ENE directions. These lineaments also define the surface boundaries of the sub-basin in accordance with late Miocene successions that crop out to the east. The lineament density map presented in this study holds potential as a valuable tool for guiding groundwater exploration in the Busaiya area. The findings suggest that the Busaiya basement sub-basin has undergone reactivation over geologic time, and it is still affected by the north and northeast drift and anticlockwise movement of the Arabian Plate that led to the development of arcuate features and differential subsidence in the southern part of the sub-basin due to the block's rotation. The Busaiya sub-basin, due to its structural and tectonic situations, may have a particular interest in mineral and hydrocarbon exploration.

Acknowledgments

The authors are highly appreciative of the Iraq Geological Survey (GEOSURV) for providing and acquiring the necessary data, documents, and software.

References

Acton, G. D., Stein, S., & Engeln, J. F. (1991). Block rotation and continental extension in Afar: A comparison to oceanic microplate systems. *Tectonics*, *10*(3), 501–526. https://doi.org/10.1029/90TC01792

Ai, H., Deniz Toktay, H., Alvandi, A., Pašteka, R., Su, K., & Liu, Q. (2024). Advancing potential field data analysis: the Modified Horizontal Gradient Amplitude method (MHGA). *Contributions to Geophysics and Geodesy*, *54*(2), 119–143. https://doi.org/10.31577/congeo.2024.54.2.1

Ai, H., Essa, K. S., Ekinci, Y. L., Balkaya, Ç., & Géraud, Y. (2024). Hunger Games Search optimization for the inversion of gravity anomalies of active mud diapir from SW Taiwan using inclined anticlinal source approximation. *Journal of Applied Geophysics*, *227*, 105443.https://doi.org/10.1016/j.jappgeo.2024.105443

Al-Amiri, H. (1979). *Structural interpretation of the Landsat Satellite Imagery for the Southern Desert of Iraq*.

Al-Ani, M. Q., & Ma'ala, K. A. (1983). *The Regional Geological Mapping of North Busaiya Area*.

Al-Bahadily, H. A., & Al-Rahim, A. M. (2024). Depth-to-Basement Estimates Using Magnetic Data of the Iraqi Southern Desert: A Statistical Approach. *IOP Conference Series: Earth and Environmental Science*, *1300*(1), 12004. https://doi:10.1088/1755-1315/1300/1/012004

Al-Bahadily, H. A., Al-Rahim, A. M., & Smith, R. S. (2024a). Determination of reactivated regions and faults in the Iraq Southern Desert with the new edge technique, inverse tilt angle of second-gradients (ITAS). *Acta Geophysica*, *72*(3), 1675–1692. https://doi:10.1007/s11600-023-01176-4

Al-Bahadily, H. A., Al-Rahim, A. M., & Smith, R. S. (2024b). Tectonic elements and structural framework deduced from magnetic data of the Southern Desert, Iraq. *Pure and Applied Geophysics*, *181*(5), 1523–1540. https://doi.org/10.1007/s00024-024-03460-w

Al-Bahadily, H. A., Fairhead, J. D., & Al-Rahim, A. M. (2024). Structural interpretation of the basement beneath the Southern Desert of Iraq based on aeromagnetic data. *Interpretation*, *12*(3), T209–T219.

Al-Gurairy, A. S. Y. (2023). The Evidences of Neotectonics Activations by using geomorphological characteristics and remote sensing, and use that in exploration of oil and gas: A case study in Al-Amghr Valley–Southern Desert of Iraq. *Al-Qadisiyah Journal For Humanities Sciences*, *26*(1), 37–56.

Al-Hashimi, H. A.-J. (1973). The sedimentary facies and depositional environment of the Eocene Dammam and Rus Formations. *J. Geol. Soc. Iraq*, *6*, 1–18.

Al-Mubarak, M. A. & Amin, R. M. (1983). *Report on the regional geological mapping of the eastern part of the Western Desert and western part of the Southern Desert*.

Al Naqib, K. M. (1967). *Geology of the Arabian Peninsula; southwestern Iraq*.

Alvandi, A., Su, K., Ai, H., Ardestani, V. E., & Lyu, C. (2023). Enhancement of potential field source boundaries using the hyperbolic domain (Gudermannian Function). *Minerals*, *13*(10), 1312. https://doi.org/10.3390/min13101312

Alvandi, A., Toktay, H. D., & Ebrahim Zadeh Ardestani, V. (2023). Edge detection of geological structures based on a logistic function: a case study for gravity data of the Western Carpathians. *International Journal of Mining and Geo-Engineering*, *57*(3), 267–274. https://doi: 10.22059/ijmge.2023.353516.595018

Aqrawi, A. A. M. (1998). Paleozoic stratigraphy and petroleum systems of the western and southwestern deserts of Iraq. *GeoArabia*, *3*(2), 229–248.https://doi:10.2113/geoarabia0302229

Bonhommet, N., Roperch, P., & Calza, F. (1988). Paleomagnetic arguments for block rotations along the Arakapas fault (Cyprus). *Geology*, *16*(5), 422–425.https://doi.org/10.1130/0091-7613(1988)016<0422:PAFBRA>2.3.CO;2

Bracey, D. R. (1968). Structural implications of magnetic anomalies north of the Bahama-Antilles Islands. *Geophysics*, *33*(6), 950–961. https://doi.org/10.1190/1.1439989

Buday, T. (1980). *The Regional Geology of Iraq, Vol. I, Stratigraphy and Paleogeography* (First). Geosurv.

Buday, T., & Jassim, S. Z. (1984). *Tectonic Map of Iraq, scale 1: 1000,000*.

Cordell, L. (1979). Gravimetric expression of graben faulting in Santa Fe country and the Espanola Basin, New Mexico. *Santa Fe Country*, 59.

Cowan, D. R., & Cowan, S. (1993). Separation filtering applied to aeromagnetic data. *Exploration Geophysics*, *24*(3–4), 429–436.https://doi:10.1071/EG993429

DeMets, C., Gordon, R. G., & Argus, D. F. (2010). Geologically current plate motions. *Geophysical Journal International*, *181*(1), 1–80.https://doi.org/10.1111/j.1365-246X.2009.04491.x

Ekwok, S. E., Eldosouky, A. M., Ben, U. C., Achadu, O.-I. M., Akpan, A. E., Othman, A., & Pham, L. T. (2023). An integrated approach of advanced methods for mapping geologic structures and sedimentary thickness in Ukelle and adjoining region (Southeast Nigeria). *Earth Sciences Research Journal*, *27*(3), 251–258.https://doi.org/10.15446/esrj.v27n3.105868

Fox, J. E., & Ahlbrandt, T. S. (2002). *Petroleum geology and total petroleum systems of the Widyan Basin and interior platform of Saudi Arabia and Iraq* (Vol. 2202). US Department of the Interior, US Geological Survey.

Horst, A. J., Karson, J. A., & Varga, R. J. (2018). Large rotations of crustal blocks in the Tjörnes Fracture Zone of Northern Iceland. *Tectonics*, *37*(6), 1607–1625. https://doi.org/10.1002/2016TC004371

Jackson, J., & Molnar, P. (1990). Active faulting and block rotations in the western Transverse Ranges, California. *Journal of Geophysical Research: Solid Earth*, *95*(B13), 22073–22087.https://doi.org/10.1029/JB095iB13p22073

Jassim, S., & Buday, T. (2006a). Tectonic Framework. In S. Z. Jassim & J. C. Goff (Eds.), *Geology of Iraq* (1st., pp. 45–56). DOLIN, sro, distributed by Geological Society of London.

Jassim, S., & Buday, T. (2006b). Units of Stable Shelf. In S. Z. Jassim & J. C. Goff (Eds.), *Geology of Iraq* (1st edition, pp. 57–70). DOLIN, sro, distributed by Geological Society of London.

Johnston, J. D., Coller, D., Millar, G., & Critchley, M. F. (1996). Basement structural controls on Carboniferous-hosted base metal mineral deposits in Ireland. *Geological Society, London, Special Publications*, *107*(1), 1–21.https://doi.org/10.1144/GSL.SP.1996.107.01.02

Le Pichon, X., & Heirtzler, J. R. (1968). Magnetic anomalies in the Indian Ocean and sea-floor spreading. *Journal of Geophysical Research*, *73*(6), 2101–2117. https://doi.org/10.1029/JB073i006p02101

Leyla, B. H., Ren, J., Zhang, J., & Lei, C. (2015). En echelon faults and basin structure in Huizhou Sag, South China Sea: Implications for the tectonics of the SE Asia. *Journal of Earth Science*, *26*(5), 690–699.https://doi.org/10.1007/s12583-015-0588-x

Long, N. N., Nguyen, D. V., Van Tran, K., & Pham, L. T. (2025). Enhancing the resolution of the edges in interpreting gravity data. *Journal of Earth System Science*, *134*(1), 33. https://doi.org/10.1007/s12040-024-02489-8

Ma'ala, K. A. (2009a). Geology of Iraqi Southern Desert, Geomorphology. *Iraqi Bull Geol Min. Special*, *7–33*.

Ma'ala, K. A. (2009b). Tectonic and structural evolution. *Geology of Iraqi Southern Desert, Special Issue of Iraqi Bulletin of Geology and Mining*, 35–52.

McCaffrey, R., Long, M. D., Goldfinger, C., Zwick, P. C., Nabelek, J. L., Johnson, C. K., & Smith, C. (2000). Rotation and plate locking at the southern Cascadia subduction zone. *Geophysical Research Letters*, *27*(19), 3117–3120.https://doi.org/10.1029/2000GL011768

Numan, N. M. S., & Bakose, G. Y. B. (1997). Lineaments: questions on the veracity of their relationships in the western and southern deserts of Iraq. *ITC Journal*, *1*(1), 41–48.

Pham, L. T., & Eldosouky, A. M. (2025). New subsurface structural insights of Northeast Vietnam: Advanced implications from high-resolution magnetic data. *Journal of Asian Earth Sciences*, *278*, 106413.https://doi.org/10.1016/j.jseaes.2024.106413

Pham, L. T., Prasad, K. N. D., Ghomsi, F. E. K., Le-Huy, M., Oliveira, S. P., Nguyen, D. V., Van Tran, K., & Do, T. D. (2025). Mapping structures obscured by sediments of the southern Hanoi basin using gravity data. *Earth Science Informatics*, *18*(3), 284. https://doi.org/10.1007/s12145-025-01809-w

Qadir, H. O., Baban, E. N., Aziz, B. Q., & Koyi, H. A. (2023). Potential field survey of subsurface structures of the NW segment of the Zagros Fold-Thrust Belt, Kurdistan Region. *Geophysical Prospecting*, *71*(8), 1673–1690.https://doi.org/10.1111/1365-2478.13401

Salem, A., Williams, S., Fairhead, J. D., Ravat, D., & Smith, R. (2007). Tilt-depth method: A simple depth estimation method using first-order magnetic derivatives. *The Leading Edge*, *26*(12), 1502–1505. https://doi:10.1190/1.2821934

Shevchenko, S. (2017). *The interpretation and integration of old seismic with new gravity data—an example from the northern Perth Basin*.

Shevchenko, S. I., & Iasky, R. P. (2004). Is there room for gravity in petroleum exploration, or is the door shut? *Exploration Geophysics*, *35*(2), 124–130. https://doi:10.1071/EG04124, 2017

Sissakian, V. K., & Deikran, D. B. (1998). *Neotectonic Map of Iraq, scale 1:1,000,000*.

Sissakian, V. K., & Fouad, S. F. A. (2012). *Geological Map of Iraq, scale 1:1000000*.

Smith, A. G. (2012). *A review of the Ediacaran to Early Cambrian ('Infra-Cambrian') evaporites and associated sediments of the Middle East*. https://doi.org/10.1144/SP366.12

Soltan, B. H. (2020). Petrology and stratigraphy of pre-Cambrian Hormuz Series outcrops in Jabal Sanam, the oldest surface rocks in Iraq. *Basrah Journal of Sciences*, *38*(3), 497–520. https://doi.org/10.29072/basjs.202039

Spector, A., & Grant, F. S. (1970). Statistical models for interpreting aeromagnetic data. *Geophysics*, *35*(2), 293–302.

Taib, H., Hadji, R., Hamed, Y., Bensalem, M. S., & Amamria, S. (2024). Exploring neotectonic activity in a semiarid basin: a case study of the Ain Zerga watershed. *Journal of Umm Al-Qura University for Applied Sciences*, *10*(1), 20–33. https://doi.org/10.1007/s43994-023-00072-3

Tamar-Agha, M. Y., & Al-Sagri, K. E. A. (2015). Shedding further light on Upper Cretaceous–Neogene subsurface lithostratigraphy of Southwestern Iraq. *Iraqi Journal of Science*, 798–827.

Valkanou, K., Karymbalis, E., Papanastassiou, D., Soldati, M., Chalkias, C., & Gaki-Papanastassiou, K. (2021). Assessment of neotectonic landscape deformation in Evia Island, Greece, using GIS-based multi-criteria analysis. *ISPRS International Journal of Geo-Information*, *10*(3), 118. https://doi.org/10.3390/ijgi10030118

Wagner, C. A. (1987). Improved gravitational recovery from a geopotential research mission satellite pair flying en echelon. *Journal of Geophysical Research: Solid Earth*, *92*(B8), 8147–8155. https://doi.org/10.1029/JB092iB08p08147

Wang, Y., Ding, Y., & Ai, H. (2022). Estimation of 2D magnetic-source parameters using analytic signals of the logarithm of different order analytic signals. *Exploration Geophysics*, *53*(3), 314–328. https://doi.org/10.1080/08123985.2021.1940945

Yamazaki, T., & Yuasa, M. (1998). Possible Miocene rifting of the Izu–Ogasawara (Bonin) arc deduced from magnetic anomalies. *Island Arc*, *7*(3), 374–382. https://doi.org/10.1111/j.1440-1738.1998.00196.x

Zaal, C., Daniilidis, A., & Vossepoel, F. C. (2021). Economic and fault stability analysis of geothermal field development in direct-use hydrothermal reservoirs. *Geothermal Energy*, *9*(1), 12. https://doi.org/10.1186/s40517-021-00193-0